Noise investigation of CW and mode-locked harmonic cavity nanolasers

YIFAN SUN,[1,2]   YANN BOUCHEREAU,[1]   SOPFY KARUSEICHYK,[1]
MATTHIEU ANSQUER,[3]   SYLVAIN COMBRIÉ,[4]   NICOLAS TREPS,[3]
ALFREDO DE ROSSI,[4]   AND FABIEN BRETENAKER[1,*]

[1]*Université Paris-Saclay, CNRS, ENS Paris-Saclay, CentraleSupélec, LuMIn, Gif-sur-Yvette, France*
[2]*Department of Information Engineering, Electronics and Telecommunications, Sapienza University of Rome, Rome, Italy*
[3]*Laboratoire Kastler Brossel, Sorbonne Université, ENS-Université PSL, CNRS, Collège de France, Paris, France*
[4]*Thales Research & Technology, Palaiseau, France*
[*]*fabien.bretenaker@universite-paris-saclay.fr*

Abstract: We theoretically investigate the noise properties of harmonic cavity nanolasers by introducing a model of coupled equations of evolution of the modes, taking spontaneous emission into account. This model is used to predict the noise among the nanolaser Hermite-Gaussian modes, both in continuous wave and mode-locked regimes. In the first case, the laser noise is described in terms of noise modes, thus illustrating the role of the laser dynamics. In the latter case, this leads to the calculation of the fluctuations of the pulse train parameters. The influence of the different laser parameters, including the amount of saturated absorption and the Henry factors, on the noise of the mode-locked regime is discussed in details.

1. Introduction

Mode-locked (ML) lasers are powerful sources for generating extremely regular optical pulse trains, which have attracted a lot of attention for many applications, such as for example material processing [1], remote sensing [2,3], or photonic signal processing [4]. From the spectral point of view, the pulse train emitted by a mode-locked laser forms an almost perfect optical frequency comb [5,6]. Such frequency combs are used for spectroscopy [7], frequency metrology [8], and quantum information [9,10]. Among possible ML laser technologies, semiconductor ML lasers are attractive because they are very compact, robust, energy efficient, and low-cost devices [11,12]. In particular, semiconductor nanolasers have attracted a lot of attention [13] due to their ultimate compactness, integrability, and energy efficiency [14].

The noise of ML lasers [15] is generally the ultimate limitation to the precision of many of their applications, such as pulse-timing measurements [16,17], displacement measurements [18], and spectroscopy [7]. Theoretical investigations of noise of ML lasers are desirable in order to minimize the noises by properly designing the lasers. For example, the noise of actively ML lasers was the first to be treated [19]. Later, soliton perturbation theory was developed and applied to additive pulse mode-locking and Kerr lens mode-locking [20], to stretched pulse fiber lasers [21], and to diode lasers [22]. A comprehensive combination of analytical and numerical techniques was also developed [23–25], which shows that perturbation theory can be applied to other types of mode-locked lasers [23,24]. Among the different ML laser noises, the carrier envelope offset (CEO) noise is the subject of particular attention [25–27] since it plays a major role in the applications of frequency combs.

Recently, a new kind of compact photonic crystal microresonator sustaining oscillation of Hermite-Gaussian (HG) modes thanks to its harmonic photonic potential has been proposed and experimentally demonstrated [28–31]. Such a resonator can be seen as the photonic analogue

of a quantum mechanical harmonic oscillator. In particular, it exhibits HG modes with evenly spaced eigenfrequencies, which is an essential requirement to achieve mode locking. A similar photonic cavity design based on effective bichromatic potential was also proposed [32], and a post-processing technique allowed the selective tuning of individual confined modes of this kind of cavity [33]. A new concept of passively mode-locked lasers has thus been proposed based on such cavities [34]. One remarkable property of such a laser is that the pulse repetition rate depends on the curvature of the photonics potential and the effective mass instead of the cavity length. Many different dynamical behaviors, similar to those observed in conventional lasers, have been discussed, such as CW oscillation, Q-switching, Q-switched mode locking, continuous-wave mode locking [35]. Robustness of mode locking to potential distortion has also been investigated by introducing some non-parabolicity and possible random errors in the shape of the photonic potential [36].

Like in all kinds of lasers, stimulated emission, which provides the gain necessary to reach laser oscillation, is also unavoidably accompanied by spontaneous emission. This spontaneous emission is at the origin of the fundamental noise limits of lasers. The aim of this paper is thus to investigate the noise properties of harmonic cavity nanolasers in the presence of spontaneous emission. Of course, lasers with nanometric dimensions are also well known to exhibit a strong Purcell effect that can enhance spontaneous emission in the laser mode [37–41], and also to exhibit peculiar noise properties, such as discretization noise, due to their small number of emitters and photons [38,42]. However, these effects are beyond the scope of the present paper, in which we stick to the simplest case in which Purcell effect is negligible and the number of photons inside the cavity is supposed to be large enough to be treated as a real random variable. This is also related to the fact that, although the technologies involved to develop the cavities we consider here fall in the domain of nanophotonics, thus partially justifying the term "nanolasers", the cavity dimensions that we consider are more in the micrometer range.

Within these hypothesis, we thus provide a general investigation of the noise properties of such a harmonic cavity nanolaser under the influence of spontaneous emission, both for CW oscillation (without any saturable absorber) and for pulsed mode locked operation. In particular, the model must take into account the peculiar spatial distribution of the field of HG modes, which is completely different from the intensity distribution of conventional standing waves. This model is then used to investigate the photon number fluctuations in each mode, total intensity noise, and the phase and frequency noises of the modes. We also put a special emphasis on the correlations between the mode fluctuations. Moreover, in the presence of a saturable absorber that ensures mode-locked operation, the different noises of the pulse train emitted by the laser, such as intensity noise, pulse duration noise, timing jitter, and phase noise, are analyzed. Their evolution, when the absorption rate and the Henry factor are varied, are also explored.

The paper is organized as follows: Section 2 introduces the laser model including the master equation, field normalization, spontaneous emission source, simulation parameters and calculation method. In Section 3, we show the special noise exchanges among HG modes by investigating the noise of photon number in each mode. Next, the different noises of the pulses created thanks to the saturable absorption are investigated. Finally, we show the influence of Henry factor on these noises. Section 4 gives the conclusions of the paper.

2. Laser model

In this section, we first describe the differential equations governing the evolution of the HG modes. The mode intensities are then normalized to be easily related to the intracavity photon number. Next, Langevin forces are introduced in the mode equations to describe spontaneous emission. Finally, the choice of parameters is discussed and the simulation method is introduced.

2.1. Master equation

As demonstrated earlier [28–31], a photonic crystal cavity can be designed to sustain HG modes with equally spaced frequencies, as shown in Fig. 1(a). In this situation, the master equation describing the evolution of the slowly-varying field envelope $A(x, t)$ has been shown to be [34–36]:

$$\frac{\partial A(x,t)}{\partial t} = -i \left[-\frac{1}{2}\omega_{kk}\partial_x^2 + \frac{\Omega^2}{2\omega_{kk}}x^2 \right] A(x,t) + H_1 A(x,t) , \qquad (1)$$

where $\omega_{kk} = \partial^2\omega/\partial k^2$ is the group velocity dispersion of the quasi-periodic photonic structure and Ω is the free spectrum range (FSR) of the harmonic cavity. The dissipative term H_1 describes three effects: i) the gain of the amplifying medium that sustains laser oscillation; ii) the saturable absorption that leads to passive mode-locking and iii) the dissipative losses of the resonator. It reads:

$$H_1 = \frac{1}{2}g(x,t)(1 - i\alpha_g) - \frac{1}{2}a(x,t)(1 - i\alpha_a) - \frac{1}{2}\gamma_0, \qquad (2)$$

where $g(x, t)$ and $a(x, t)$ are the space and time dependent gain and saturable absorber rates, with their respective Henry factors α_g and α_a. The term γ_0 holds for the intrinsic losses.
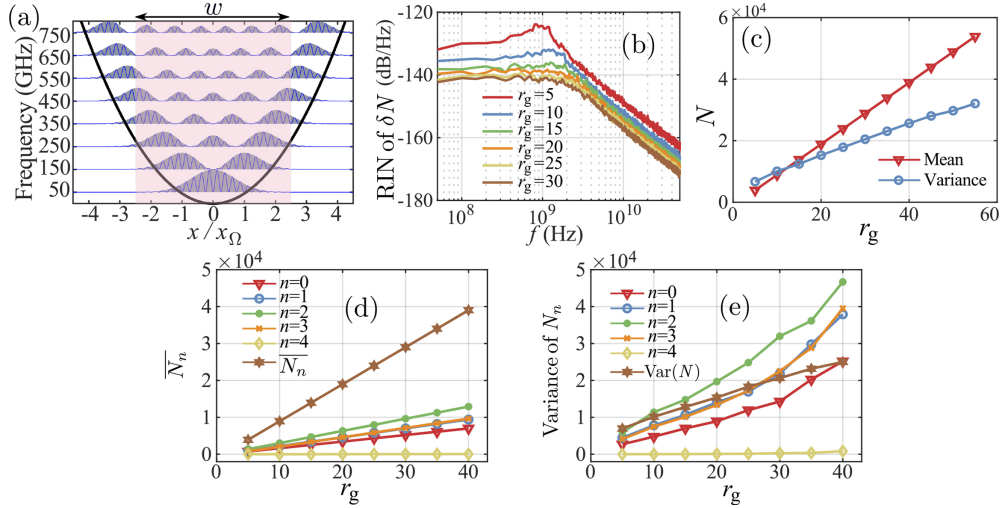

Fig. 1. (a) Shape of the HG modes within the parabolic potential. The semitransparent pink area represents the active medium with width $w = 5x_\Omega$, containing both gain and/or saturable absorption. (b) RIN of the total number of photons N for different values of the relative gain parameter $r_g = g_0/\gamma_0$. (c) Mean and variance of N as a function of r_g. (d) Mean value and (e) variance of the photon numbers N_n in mode n as a function of r_g. There is no saturable absorption in this case: $r_a = a_0/\gamma_0 = 0$.

The field envelope $A(x, t)$ can then be expanded on the basis of the HG modes of the resonator:

$$A(x,t) = \sum_{n=0}^{\infty} C_n(t)e^{-i\Omega_n t}\Psi_n(x), \qquad (3)$$

where the $C_n(t)$'s are the complex coefficients of this expansion and where the longitudinal coordinate x has been re-normalized to the scaling factor

$$x_\Omega = \sqrt{\omega_{kk}/\Omega}. \qquad (4)$$

The amplitude of the HG mode $\Psi_n(x)$ is then given by:

$$\Psi_n(x) = \frac{1}{\sqrt{2^n n!}} \pi^{-1/4} \exp\left(-x^2/2\right) H_n(x) \ , \tag{5}$$

with H_n is the Hermite polynomial of order n. The corresponding eigenfrequency is

$$\Omega_n = \left(n + \frac{1}{2}\right) \Omega \ . \tag{6}$$

Substituting Eq. (3) into Eq. (1), and projecting on the HG modes leads to a set of equations of evolution for the mode amplitudes C_n:

$$\frac{dC_n(t)}{dt} = M_n(t), \tag{7}$$

where

$$M_n(t) = e^{i\Omega_n t} \int_{-\infty}^{+\infty} H_1 A(x, t) \Psi_n(x) dx. \tag{8}$$

2.2. Field normalization

In the following, we normalize the complex field envelope $A(x, t)$ in such a way that $|A(x, t)|^2$ is equal to the energy density $E_D(x, t)$ along x:

$$E_D(x, t) = |A(x, t)|^2. \tag{9}$$

Then the photon density per unit length along the x axis is easily expressed as

$$N_D(x, t) = E_D(x, t)/\hbar\omega_0 = |A(x, t)|^2/\hbar\omega_0 \ , \tag{10}$$

where ω_0 is the light carrier frequency and where $N_D(x, t)$ is the photon density. Therefore, the total field energy inside the cavity is

$$E(t) = \int_{-\infty}^{\infty} |A(x, t)|^2 dx = \sum_{n=-\infty}^{\infty} |C_n(t)|^2 \ , \tag{11}$$

where the energy in mode n is

$$E_n(t) = |C_n(t)|^2. \tag{12}$$

Moreover, the photon number in mode n is

$$N_n(t) = |C_n(t)|^2/\hbar\omega_0, \tag{13}$$

and the total photon number in the laser is

$$N(t) = \sum_{n=-\infty}^{\infty} |C_n(t)|^2/\hbar\omega_0. \tag{14}$$

The equation of evolution (7) of the mode amplitudes is coupled to equations governing the saturation of the gain and of the saturable absorber. Saturation of the gain is described according to

$$\frac{\partial g(x, t)}{\partial t} = -\frac{g(x, t) - g_0(x)}{\tau_g} - \frac{N_D(x, t)}{N_{sat,g}\tau_g} g(x, t) \ , \tag{15}$$

where $g_0(x)$ is the unsaturated gain rate, τ_g is the gain lifetime, and where $N_{sat,g}$ is the saturation photon density for the gain medium. To evaluate the value of $N_{sat,g}$, we suppose that the typical

photon number inside the cavity, which is of the order of $N_{\text{sat,g}}L$ when the laser is a few times above threshold, is of the order of 1000. This corresponds to a dissipated power of 1μW if the intrinsic losses are equal to $\gamma_0 = 10^{10}\,\text{s}^{-1}$. As we will see in the next section, the cavity lengths L that we consider are of the order of $50\,\mu$m. Therefore, we take in the following a saturation photon density equal to $N_{\text{sat,g}} = 2 \times 10^7\,\text{m}^{-1}$, which is of the same order of magnitude as in conventional semiconductor lasers [43].

Saturation of the absorption coefficient $a(x, t)$ is governed by an equation similar to Eq. (15), with a saturation photon density $N_{\text{sat,a}}$, and absorber lifetime τ_a, and an unsaturated absorption density $a_0(x)$. In the following, the saturation of the absorber is related to the gain saturation by the saturation energy ratio:

$$R_{\text{E}} = \frac{N_{\text{sat,g}}\tau_{\text{g}}}{N_{\text{sat,a}}\tau_{\text{a}}} \, . \tag{16}$$

2.3. Spontaneous emission

As mentioned in the introduction, we treat the photon number as a continuous real variable, and thus describe the spontaneous emission falling into each HG mode n by a Langevin force $S_n(t)$ added to Eq. (7), which thus becomes:

$$\frac{\mathrm{d}C_n(t)}{\mathrm{d}t} = M_n(t) + S_n(t) \, . \tag{17}$$

Spontaneous emission is modeled by a complex Gaussian white noise obeying [44]

$$<S_n(t)> = 0, \tag{18}$$

$$<S_n(t)S_n^*(t-\tau)> = (R_{\text{sp},n}/2)\delta(\tau) \, , \tag{19}$$

where $<>$ holds for the ensemble average and $\delta(t)$ is the Dirac function and where $R_{\text{sp},n}$ is the spontaneous emission rate for mode n.

In the rest of the paper, we use Eq. (17) to simulate the laser mode evolution in the presence of spontaneous emission whose characteristics are given in Eqs. (18,19). To perform such simulations, time needs to be discretized with a step duration ΔT. The Langevin force is then replaced by its discretized version:

$$S_n(t) = \chi\sqrt{R_{\text{sp},n}/(2\Delta T)} \, , \tag{20}$$

where χ is a complex Gaussian random variable with zero mean and unit variance.

The spontaneous emission rate per atom is equal to the stimulated emission rate in the presence of one photon in the mode. Taking into account the fact that around steady-state the saturation gain per round-trip compensates for the losses, the rate of spontaneous emission into mode n is then equal to the intrinsic losses [45]:

$$R_{\text{sp},n} = \gamma_0. \tag{21}$$

This expression leads to the same order of magnitude as the one calculated for conventional semiconductor lasers and based on the evaluation of the threshold carrier density [43].

2.4. Parameters

The values of the parameters used in the simulations are given in Table 1.

Table 1. Values of the parameters used in the simulations.

Item	Notation	Value	Unit	References
FSR	$\Omega/2\pi$	100	GHz	
Scaling length	x_Ω	8.4	μm	
Gain width	w	$5\,x_\Omega$		
Gain lifetime	τ_g	1	ns	[46,47]
Absorber lifetime	τ_a	10	ps	[46,48,49]
Intrinsic loss rate	γ_0	10^{10}	1/s	
Saturation photon density of the gain	$N_{sat,g}$	2×10^7	1/m	
Saturation ratio between gain and absorber	R_E	25		[48]
Spontaneous emission rate	$R_{sp,n}$	$= \gamma_0$	1/s	[45]

2.5. Numerical method

The mode equations of evolution (Eq. (17)) are stochastic differential equations, which can be numerically solved using Euler's method [50]. To improve the accuracy in the resolution of the deterministic part $dC_n(t) = M_n(t)dt$ of Eq. (17), we use the standard Runge-Kutta method (RKM) with a fixed time-step $\Delta T = 10$ fs. A random value of the Gaussian variable $S_n\Delta T$ is added to the output of the RKM iteration at every time step. In this way, we compute the time evolution of each mode amplitude $C_n(t)$ for 50 ns. Since the time to reach steady-state is generally shorter than 10 ns [35], the data within the last 25 ns can be used to analyze the steady-state regime of operation of the laser. Therefore, the fluctuations of the different laser parameters are extracted from this integration period in the rest of the paper.

3. Results

In this section, we first consider the CW laser oscillation regime obtained in the absence of saturable absorber inside the cavity ($a_0(x) = 0$). In particular, we put emphasis on the role of mode competition in the intensity fluctuations of the different resonator modes, leading to the appearance of noise modes. In the second subsection, an intracavity saturable absorber is supposed to be present ($a_0(x) \neq 0$), leading to the study of the laser noise in pulsed ML regime. Finally, the influence of the Henry factor on the pulsed laser noise is investigated.

3.1. Noise modes in CW oscillation regime

As stated above, we start with the simplest case where the laser contains no saturable absorber ($a_0 = 0$) and thus oscillates in CW regime. We then first investigate the noise of the total intracavity photon number $N(t)$, and in particular its evolution with the laser gain. It can be calculated using Eqs. (13,14) and the numerically computed mode amplitudes $C_n(t)$ in steady-state. We then separate its average value $\overline{N}$ and fluctuation $\delta N(t)$:

$$N(t) = \overline{N} + \delta N(t). \tag{22}$$

The power spectrum density (PSD) $S_{\delta N}(f)$ of these fluctuations is given by

$$S_{\delta N}(f) = |\delta N(f)|^2, \tag{23}$$

where $\delta N(f)$ is the Fourier transform of $\delta N(t)$. Numerically, it is evaluated using a Hann window. The relative intensity noise (RIN) spectrum is then obtained as

$$\text{RIN}(f) = \frac{S_{\delta N}(f)}{\overline{N}^2}. \tag{24}$$

In the following, our simulations are limited to the 10 first HG modes. Moreover, the RIN and PSD spectra are averaged over 60 independent runs of the simulation using the same parameters but independent drawings of the spontaneous emission noise. This averaging process will also be used in the following sections to evaluate the noise of other laser parameters.

As a first example, the RIN spectrum for the total photon number is shown in Fig. 1(b) for different values of the relative gain $r_g = g_0/\gamma_0$. We observe that the relaxation oscillation peak around $1 \sim 2$ GHz decreases and shifts to higher frequencies when the gain is increased. The RIN also decreases, because the average photon number $\overline{N}$ increases with increasing gain. This can be seen in Fig. 1(c). The evolution of the variance of N is also plotted in the same figure. It is obtained by integrating the PSD of $\delta N(f)$ over the frequency range $[0.12\,\text{GHz}, 50\,\text{GHz}]$. Since the noise variance increases with the gain slower than $\overline{N}$, the relative intensity noise decreases with g_0.

More physical insight can be gained in the laser behavior by investigating the fluctuations of the photon numbers $N_n(t)$ in each individual HG mode n, which are derived from the C_n 's using Eq. (13). Their mean values $\overline{N_n}$ are plotted as a function of r_g in Fig. 1(d). With the gain window width we have chosen ($w = 5\,x_\Omega$), only the first four modes ($n = 0, 1, 2, 3$) contribute. The evolution of the variances of the N_n's is reproduced in Fig. 1(e). Contrary to the variance of N, the variances of the N_n's increase with r_g faster than their average values. Moreover, one notices that the variance of the fluctuations of N_2, the number of photons in mode $n = 2$, is even larger than the variance of the total photon number N. We thus expect that there exist strong correlations between the photon numbers in the different HG modes.

A first insight in these correlations can be gained by simply looking at the time evolution of the number of photons in the laser modes, as displayed in Fig. 2(a). For example, by comparing the fluctuations of N_0 and N_1, or the fluctuations of N_3 and N_4, it seems that adjacent mode exhibit anti-correlated fluctuations, which is consistent with the fact that competition between adjacent modes dominates the dynamics of such lasers based on HG modes [35].

A more quantitative investigation of these correlations is proposed in Figs. 2(b-h). First, Fig. 2(b) reproduces the PSD of the δN_n's, together with the PSD of δN. The corresponding variances are given as an inset. One can notice that the PSDs of the individual modes are larger than the PSD for the total photon number for frequencies $f < 0.5$ GHz. This is another proof that there exist negative correlations between the fluctuations of the different modes.

To better understand why the fluctuations of the total photon number are lower than those of the individual modes, we define the noise correlation matrix $\mathbf{M}(f) = [M_{mn}(f)]$ as

$$M_{mn}(f) = \langle \delta N_m(f) \delta N_n^*(f) \rangle \,, \tag{25}$$

where $\delta N_m(f)$ is the Fourier transform of $\delta N_m(t)$ using the Hann window and where $\langle \cdot \rangle$ holds for averaging over many independent simulations (60 in the present case). The diagonal elements of this matrix are the PSDs of the photon number fluctuations for the individual modes while the non-diagonal elements provide information on noise correlations between different modes.

The modulus $|M_{mn}|$ of the matrix at $f = 0.2$ GHz is shown in Fig. 2(c). The diagonal elements are larger than the others. However, the non-diagonal elements of $|M_{mn}|$ are also large, especially for the elements close to the diagonal. Such a noise matrix is very similar to the mode saturation matrix of HG modes [35] due to their quite localized spatial distribution. It confirms the fact that the competition between two HG modes labeled by integers n and m is relatively strong when $|m - n| = 1$ and then progressively decreases for larger values of $|m - n|$. On the contrary, the matrix $|M_{mn}|$ at $f = 2$ GHz (Fig. 2(d)) is very different from the preceding one. The noise correlations between the modes are very weak here. Only the diagonal elements are significant.

The diagonal elements are real, and the phases of the correlations between the modes are directly given by the arguments of the corresponding non-diagonal elements. Figures 2(e-h) reproduce the evolution of the argument of M_{mn} as a function of f. The values for $m = 0$ are
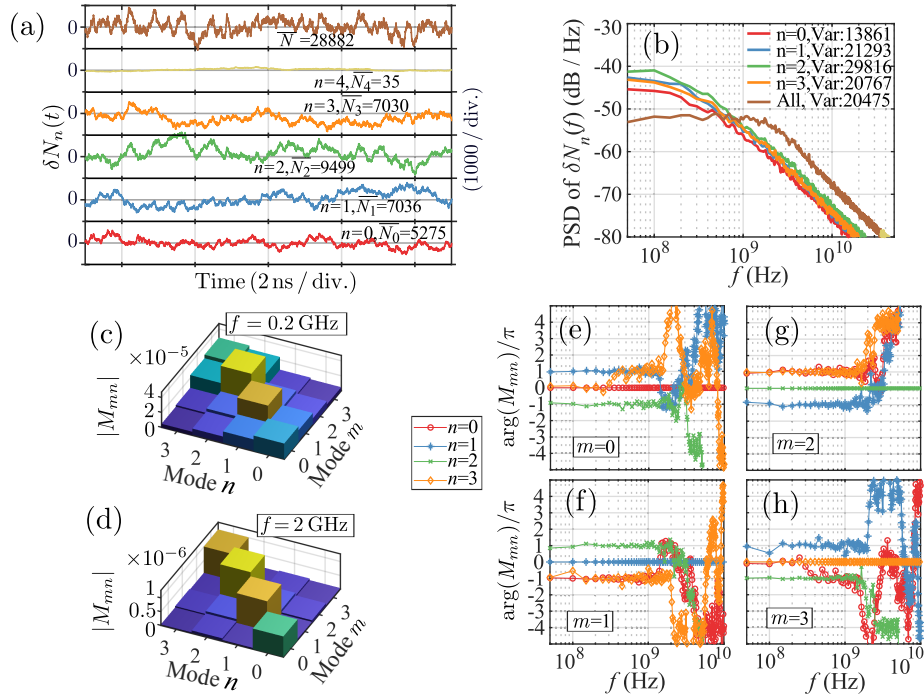
Fig. 2. (a) Example of time evolution of the photon number fluctuations $\delta N_n(t)$ for individual modes and $\delta N(t)$ for all modes. (b) Corresponding PSDs. (c,d) Modulus of the noise correlation matrix for (c) $f = 0.2$ GHz and (d) $f = 2$ GHz. (e-h) Phases $\arg(M_{mn})$ of noise correlation matrix elements versus f. Other parameter values are $r_g = g_0/\gamma_0 = 30$, $r_a = a_0/\gamma_0 = 0$.

shown in Fig. 2(e). They indicate that the fluctuations of modes $n = 1, 2$ are in antiphase with respect to those of mode $m = 0$ for frequencies $f < 1$ GHz. As the difference in mode order increases, the anti correlation is no longer obvious. For example, the fluctuations of mode $n = 3$ are in phase with those of mode $m = 0$ for $f < 0.3$ GHz. In the region $f > 1$ GHz, the correlations between modes vanish and their phases thus become meaningless. The cases $m = 1, 2, 3$ shown in Figs. 2(f-h) follow similar behaviors as $m = 0$ shown in Fig. 2(e). For example, the fluctuations of mode $m = 1$ (or $m = 2$) are negatively correlated to those of their neighbouring modes.

Further insight can be gained into these noise correlations by deriving the eigenmodes of the noise correlation matrix $\mathbf{M}(f)$ at a given frequency f. Figure 3(a) plots the eigenvalues λ_i of $\mathbf{M}(f)$ as a function of f. These eigenvalues λ_i correspond to the PSDs of the noise modes.

The four corresponding eigenvectors $\mathbf{e}_i$, $i = 0..3$, represent the four main energy exchange mechanisms among the HG modes at a given frequency. Each eigenvector has four complex components among the four considered HG modes, i.e., $\mathbf{e}_i = \sum_{j=0}^{3} e_{ij}\Psi_j$. The four complex components e_{ij} for each eigenvector i are plotted as arrows in the complex plane in Fig. 3(c) for $f = 0.2$ GHz. The noise mode that carries the largest noise power is mode $i = 0$. We can see from Fig. 3(c) that this mode corresponds to an exchange of photons between mode 2 on the one hand and modes 1 and 3 on the other hand. This is consistent with the fact that neighbouring modes should exhibit anticorrelated intensity fluctuations. Noise mode $i = 1$ corresponds to photon exchanges between mode 1 on the one hand and modes 0 and 3 on the other hand. Mode $i = 2$ corresponds mainly to competition between modes 0 and 3. Finally, mode $i = 3$ corresponds to a noise mode commmon to all the HG modes, but is completely negligible compared to the other
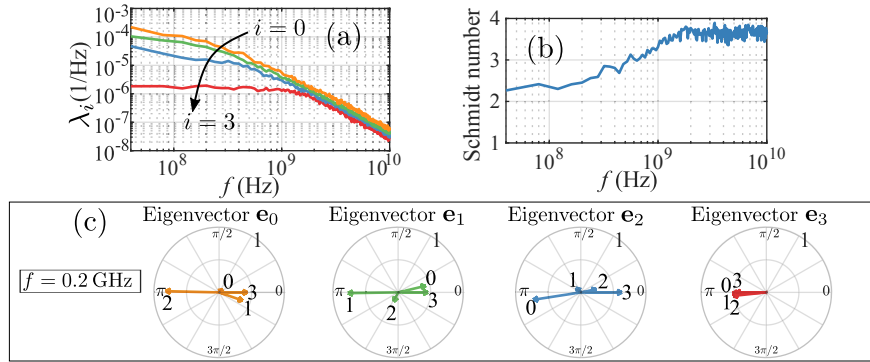
Fig. 3. (a) Eigenvalues of the noise correlation matrix and (b) Schmidt number K as a function of frequency. (c) Complex representation of the four components e_{ij} of the four eigenvectors $\mathbf{e}_i$ of the noise matrix for $f = 0.2\,\text{GHz}$, Other parameter values are $r_g = g_0/\gamma_0 = 30$, $r_a = a_0/\gamma_0 = 0$.

noise modes ($\lambda_3 \ll \lambda_0, \lambda_1, \lambda_2$ at low frequencies). The fact that this noise mode is negligibly small compared to the three other ones can also be seen by looking at the Schmidt number [51] of this expansion, given by

$$K = \frac{(\sum_i \lambda_i)^2}{\sum_i \lambda_i^2}. \tag{26}$$

This number quantifies the number of eigenmodes that significantly contribute to the physical process described by the noise matrix. In our case, its evolution with frequency, shown in Fig. 3(b), shows that only two to three modes significantly contribute to the laser noise at frequencies lower than 0.5 GHz. A similar behavior is obtained when more modes are made to contribute to the laser operation by increasing the gain width w, as shown in the Supplemental.

3.2. Noise of ML laser

In this subsection, we suppose that a saturable absorber is now also introduced inside the cavity. It has the same width as the gain and is also located in the center of the cavity (pink region in Fig. 1(a)). This absorber leads to mode-locked pulsed laser operation [34]. For such a solution, we analyze the mode noises in a manner similar to the preceding subsection. Further, this also leads to the investigation of the noise of the pulse train emitted by the laser.

3.2.1. Noise properties of the locked modes

The first interesting point is how the photon number noise evolves with the amount of saturable absorption. By using the same methods as in the preceding subsection, the PSDs of the total photon number for different values of the relative absorption $r_a = a_0/\gamma_0$ are shown in Fig. 4(a). As the absorption increases, the amplitude of the relaxation oscillation peak increases. The frequency of this peak shifts towards lower frequencies. As previously investigated [35], when $r_a = a_0/\gamma_0$ increases from 0, the laser operation regime evolves from multimode unlocked operation, to CW mode locking, then to Q-switched mode locking, and finally to passively Q-switched regime. For example, the intensity noise spectra in Fig. 4(a) correspond to CW mode-locking for $r_a = 1.0$ to 6.0. Above this value, the relaxation oscillations do not longer damp, leading to Q-switched mode-locking [52], as shown by the spectrum corresponding to $r_a = 7.0$. This explains why the PSD of the intensity fluctuations is much stronger in this case.

In order to try and minimize the mode-locked laser intensity fluctuations, we calculate the variance of this noise by integrating the PSD of N over the bandwidth $(0.12\,\text{GHz}, 50\,\text{GHz})$. The
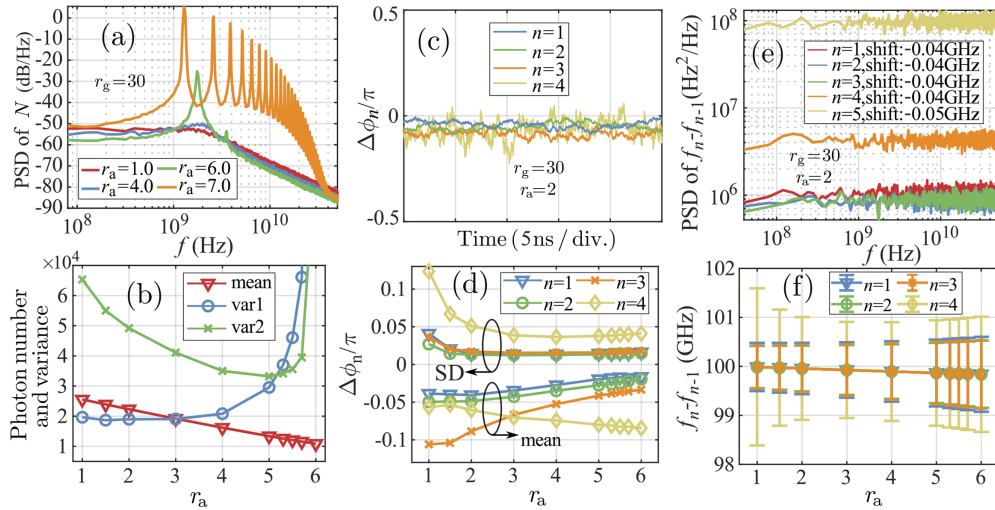
Fig. 4. (a) PSD of the fluctuations in total photon number N for different values of relative absorption $r_a = a_0/\gamma_0$. (b) Evolution of the mean value and variance (labeled "var1") of the total photon number versus r_a. The plot labeled "var2" is the sum of the variances of the photon numbers in each mode. (c) Time evolution of the mode phase differences $\Delta\phi_n = 2\phi_n - \phi_{n-1} - \phi_{n+1}$. (d) Mean and standard deviation (SD) of $\Delta\phi_n$ as a function of r_a. (e) PSD of mode frequency separations $f_n - f_{n-1}$. The shifts with respect to the cold cavity FSR of $100\,\text{GHz}$ are given in the insert. (f) Mode frequency separation $f_n - f_{n-1}$ as a function of r_a. The length of the error bar represents the value of the SD. In this figure, $r_g = g_0/\gamma_0 = 30$.

evolution of this variance with r_a is plotted with blue circles in Fig. 4(b). When one increases the amount of saturable absorption, this variance initially slightly decreases, before strongly increasing for $r_a = a_0/\gamma_0 > 2$. This shows that the value of r_a should be chosen to be large enough to stabilize mode-locked operation but should not be too large in order to avoid enhancing the noise at the relaxation oscillation frequency.

We then compare the variance of the fluctuations of the total photon number N (blue circles in Fig. 4(b)) with the sum of the variances of the photon numbers N_i of the individual modes, (green crosses in Fig. 4(b)). Clearly, a large part of the noise of individual modes corresponds to exchange of photons with the other modes, like in the case of CW operation. This similarity with the CW regime is also shown by the analysis of the noise correlation matrix of the HG modes, which is performed in Section 2 of the Supplemental. Here, in mode-locked regime, the importance of the noise in photon number is reduced by increasing the absorption. However, the price to pay is a reduction of the average number of photons in the laser (see the red triangles in Fig. 4(b)).

Mode-locked operation relies on the locking of the relative phase between the modes. We thus plot in Fig. 4(c) one example of the time evolution of the phase differences $\Delta\phi_n = 2\phi_n - \phi_{n+1} - \phi_{n-1} = 0$ between three successive modes, where $\phi_n(t)$ is the phase of $C_n(t)$. This example has been obtained for $r_g = 30$ and $r_a = 2$. One can see that in spite of the fluctuations induces by spontaneous emission, the laser modes remain locked. Moreover, one notices that $\Delta\phi_n$ fluctuates much more for $n = 4$ than for $n = 1, 2, 3$. This is due to the relatively lower power of mode $n = 5$.

This can be seen more quantitatively by plotting the mean value and the standard deviation (SD) of $\Delta\phi_n$ as a function of $r_a = a_0/\gamma_0$, as shown in Fig. 4(d). The SDs for all values of n start decreasing for low values of r_a, reach a minimum in the vicinity of $r_a \simeq 2$, and then increase. The

mean values of all $\Delta\phi_n$'s approach 0 as the absorption increases, except for $n = 4$. Increasing the absorption thus provides a stronger locking, leading to $\Delta\phi_n$ closer to 0 on average and exhibiting less noise. But a too large value of the absorption is not favorable as it brings the laser closer to Q-switched operation.

An alternative view of the influence of saturable absorption and spontaneous emission on the stability of mode locking can be obtained by looking at the mode frequency separation. The instantaneous frequency shift f_n of mode n with respect to the carrier optical frequency ω_0, is the time derivative of its phase:

$$f_n = \frac{1}{2\pi}\left(\Omega_n - \frac{d\phi_n}{dt}\right). \tag{27}$$

We then plot the PSD of the instantaneous mode frequency separation $f_n - f_{n-1}$ in Fig. 4(e). This frequency noise is white in the considered frequency domain, as expected from the characteristics of spontaneous emission. Similarly to phase noises, higher order modes ($f_n \geq 4$) exhibit stronger frequency noises because they have less power. It is worth noticing that the mode frequency separations are reduced by approximately -0.04 GHz compared to the cold cavity free spectral range (FSR). Further investigation of the mode separation $f_n - f_{n-1}$ as a function of $r_a = a_0/\gamma_0$ is shown in Fig. 4(f). This plot shows the mean value of $f_n - f_{n-1}$ together with its standard deviations corresponding to the length of the error bars. One can see that the mean value of the frequency separation $f_n - f_{n-1}$ is the same for all modes n, due to stable mode-locked operation. Moreover, it slightly decreases as r_a increases. This frequency pulling effect is due to the finite recovery time of the saturable absorber. This leads to time asymmetric losses for the pulse when it crosses the absorber: the leading edge of the pulse is more strongly attenuated than its tail, so that the pulse center is slightly delayed. This explains this decrease of the pulse repetition rate. As this pulling of the mode separation increases, the noise in the mode separation slightly increases, except for $n = 4$ (see Fig. 4(f)) when $r_a < 3$.

3.2.2. Noise properties of the laser pulse train

Just like any ML laser, the nanolasers we consider here need some output coupling mechanism to emit a pulse train. For simplicity here, we suppose that this output coupling occurs at $x = 0$. We thus suppose that the field at the laser output is proportional to $A_+(x = 0, t)$ propagating in $+x$ direction at cavity center ($x = 0$). The fields $A_+(x, t)$ can be derived from $A(x, t)$ using the following steps: (1) $A(x, t)$ is Fourier-transformed to $A(k, t)$ in k-space; (2) only the part of the field $A(k, t)$ with $k > 0$ is kept and transformed back to $A_+(x, t)$ in real space.

In order to study the emitted pulse train, we focus on the quantity $N_+(t) = |A_+(t)|^2 x_\Omega$, where x_Ω is the scaling factor in Eq. (4), because it is dimensionless and related to the photon number inside the laser. In steady-state CW ML operation and in the absence of spontaneous emission, the peak value N_p of $N_+(t)$ does not depend on time. But the introduction of spontaneous emission in our model makes it vary from pulse to pulse and thus introduces some time dependence noted $N_p(t)$. The relative noise of $N_p(t)$, defined as the PSD of its fluctuations divided by the square of its average value, is plotted in Fig. 5(a) for several values of r_a. Increasing the absorption leads to an increase of the relaxation peak around 2 GHz. This is reminiscent of what we observed in Fig. 4(a) for the noise of the total photon number. This also explains why the relative variance of N_p, which is the integral of the relative noise spectrum over the entire frequency band, increases with r_a, as evidenced by the blue open circles in Fig. 5(b). However, the red triangles in the same figure, which represent the evolution of the variance of N_p, show that a part of this increase has to be attributed to the decrease of the mean value of N_p induced by the increase of the absorption.

The (full-width at half maximum) pulse duration Δt also fluctuates from pulse to pulse because of spontaneous emission noise. We thus plot the PSD of the fluctuations of Δt for increasing values of r_a in Fig. 5(c). Again, the stabilization of the pulse train obtained for small values of r_a can be seen by the reduction of the noise of Δt for $r_a = 2$ compared to $r_a = 1$. But, here again,
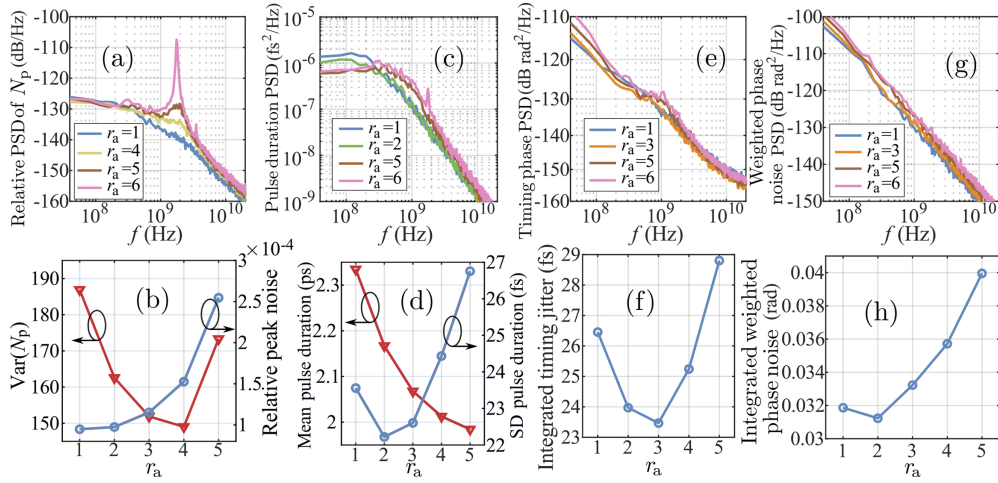
Fig. 5. (a) Relative PSD of the pulse peak N_p. (b) Variance of N_p and relative peak noise $\text{var}(N_\text{p})/(\overline{N_\text{p}}^2)$ of pulse peaks as a function of $r_\text{a} = a_0/\gamma_0$. (c) PSD of the pulse duration Δt. (d) Mean value and standard deviation (SD) of Δt versus r_a. (e) PSD of the timing phase noise of the pulses. (f) Corresponding timing jitter as a function of r_a. (g) PSD of the weighted phase noise. (h) Integrated weighted phase noise as a function of r_a. The integration frequency range for (b,d,f,h) is [0.12 GHz, 50 GHz]. In this figure $r_\text{g} = g_0/\gamma_0 = 30$.

the noise increases at frequencies around the relaxation oscillation frequency when one increases r_a in such a way that the laser becomes close to Q-switched ML operation (see the spectra for $r_\text{a} = 5$ and 6 in Fig. 5(c)). This is confirmed by the evolution of the SD of the pulse duration noise reported in Fig. 5(d) (blue open circles). Notice also that an increase of the amount of saturable absorption reduces the average pulse duration.

The timing jitter noise of the pulses is an important parameter for applications such as optical clocking. To derive it, we first calculate the noise of the instantaneous repetition rate [23]. The fluctuation of the instantaneous repetition frequency is

$$\delta f_{\text{rep},n} = \frac{1}{T_n} - \frac{1}{\overline{T}}, \tag{28}$$

where T_n is the duration between the peaks of two successive pulses labeled by $n - 1$ and n, and $\overline{T}$ is the mean value of T_n. The PSD $S_\phi(f)$ of the timing phase noise is related to the PSD $S_{f_{\text{rep}}}(f)$ of the instantaneous repetition frequency through [23]

$$S_\phi(f) = \left(\frac{1}{f}\right)^2 S_{f_{\text{rep}}}(f). \tag{29}$$

Finally the PSD of the timing jitter noise is given by

$$S_{\delta T}(f) = \left(\frac{\overline{T}}{2\pi}\right)^2 S_\phi(f). \tag{30}$$

The PSD of the timing phase noise for different amounts of saturable absorption is shown in Fig. 5(e). By calculating the square root of the integral of the timing jitter PSD, we obtain the integrated timing jitter, whose evolution as a function of $r_\text{a} = a_0/\gamma_0$ is reproduced in Fig. 5(f). An increase of the absorption reduces the pulse timing jitter as long as $a_0/\gamma_0 \leq 3$, and then increases it due to the mode locking instability.

With the same data, we can also investigate the phase noise of the pulse train. Since the nanolasers that we consider emit relatively long pulses (typically 2 ps), that correspond to the oscillation of only a few HG modes, the CEO phase noise [53] is not a relevant quantity [25,54]. In order to characterize the laser phase noise, we thus choose to focus on the average of the phase noises of the HG modes weighted by their average numbers of photons. This leads to the definition of the weighted frequency fluctuation as

$$\delta f_{\mathrm{w}}(t) = \frac{1}{\overline{N}} \sum_n \overline{N_n} \delta f_n(t), \tag{31}$$

where $\delta f_n(t)$ holds for the fluctuations of frequency f_n of Eq. (27) and the sum runs over all oscillating HG modes. In the following examples we take $n = 0, \dots, 10$. The weighted phase noise PSD is then obtained as

$$S_{\phi_{\mathrm{w}}}(f) = \frac{1}{f^2} S_{\delta f_{\mathrm{w}}}(f). \tag{32}$$

The spectra of this weighted phase noise are shown in Fig. 5(g,h). This phase noise is actually quite small. And its value is similar to the one that is obtained by another method consisting in monitoring the phase of $A_+(0, t)$ at every peak of the intensity, as shown in the Supplemental. However, this phase noise is approximately 60 dB smaller than the CEO phase noise that could be expected from the timing jitter phase noise of Fig. 5(e).

Obviously, the weighted phase noise is related to the modal frequency noise. It is minimal at $r_{\mathrm{a}} = 2$ because the mode frequency noise $n = 4$ in Fig. 4(f) also reaches a minimum. The noises of all mode frequencies increase when $r_{\mathrm{a}} > 2$ due to the frequency pulling due to absorption, leading to an increase of the weighted phase noise.

3.2.3. Pulse noise behavior in the presence of a Henry factor

The same process can be used to investigate the influence of the Henry factors α_{g} of the gain medium and α_{a} of the absorber on the different noises. As a difference in the values of the Henry factors for the gain medium and the absorber is detrimental to mode locking [36,55,56], we focus here on the case where they are equal, i. e., $\alpha \equiv \alpha_{\mathrm{g}} = \alpha_{\mathrm{a}}$. Furthermore, we fix the values of the relative gain rate $r_{\mathrm{g}} = 30$ and relative absorption rate $r_{\mathrm{a}} = 1$.

The results of the simulations show that the Henry factors do not affect the noise level of the total number of photons but modify the noises of the photon numbers of individual modes. The details of these results for different values of the Henry factors can be seen in the Supplemental. The result of that is a change in the noise of the pulse peak intensity at the laser output. One example of this phenomenon can be seen in Fig. 6(a). As the Henry factor increases, a peak in the RIN at abound 0.5 GHz appears in the PSD of N_{p}, while its low frequency noise decreases. This peak gives rise to the increase in total intensity noises of pulses, as can be seen as blue circles in Fig. 6(c).

By using the same methods as in Fig. 5(c,d,f,h), the evolutions of the four kinds of noises of the pulse train (peak number of photons, duration, timing jitter, and phase) with increasing values of α are plotted as open circles connected by a solid blue line in Figs. 6(c-f). In general, a large Henry factor increases the noise level of all these four quantities. Notice also that the mean value of the pulse duration slightly reduces when α increases (see Fig. 6(d)).

To simplify the implementation of such lasers, it might be helpful to separate the gain and absorber regions [35], as shown in Fig. 6(b). A sketch of a structure in which these two regions are separated is shown in Fig. 6(b). The gain area is represented by the semitransparent red region on the left side $(-2.5x_\Omega, 0)$ while the absorber is represented by the semitransparent green region on the right side $(0, -2.5x_\Omega)$. In the absence of noise, the solutions for this spatially separated scheme are very close to those for the overlapped scheme [35]. As far as the influence of the Henry factor on the noise is concerned, we represent the results for the structure of Fig. 6(b) as
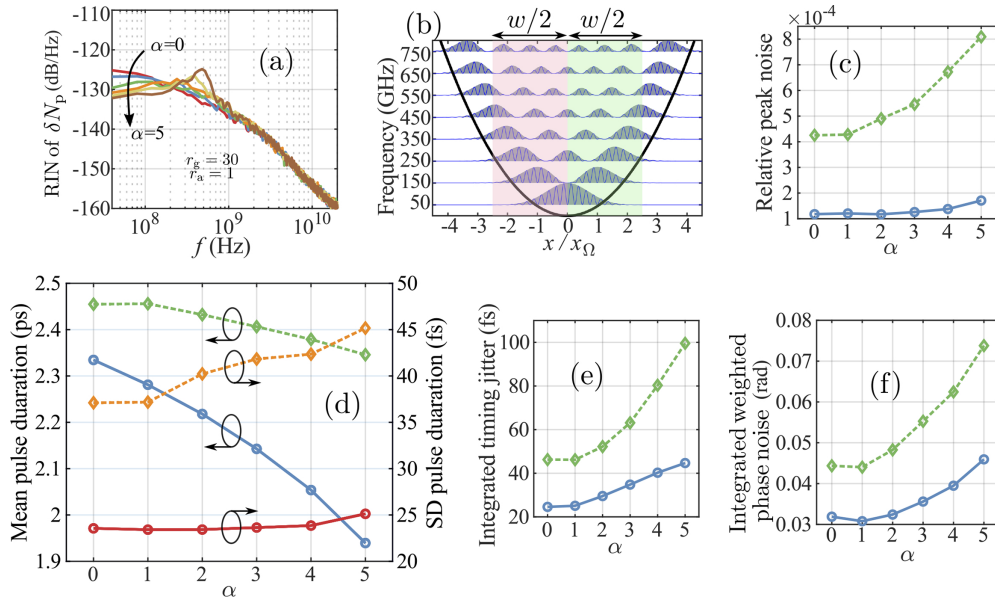
Fig. 6. (a) RIN of intensity at pulse peak for different values of the Henry factors α. (b) Laser structure with spatially separated gain (red region $-2.5x_\Omega \leq x \leq 0$) and absorber green region between $0 \leq x \leq 2.5x_\Omega$). (c-f) Laser noise evolution versus α. Open circles linked by blue solid line: overlapped scheme of Fig. 1(a); open diamonds linked by dashed green line: separated scheme of Fig. 6(b). (c) Relative peak intensity noise. (d) Mean value and SD of pulse duration. (e) PSD of timing phase. (e) Integrated timing jitter. (f) Integrated weighted phase noise. Integration bandwidth is $[0.12\,\text{GHz}, 50\,\text{GHz}]$. $r_\text{g} = 30$, $r_\text{a} = 1$.

green open diamonds connected by a dashed line in Figs. 6(c,d,e,f). Because the gain region is twice smaller in this case, the laser power is smaller [35] and the amplitudes of the different noises are larger. But the general tendency for the noise evolution with the Henry factor is similar in both cases.

4.　Conclusions

In conclusion, we have theoretically analyzed the different noise properties of harmonic cavity nanolasers in the presence of spontaneous emission. In our model, the spontaneous emission falling into a given laser mode is modeled as a Langevin force introduced in the differential equation governing the mode complex amplitude.

This model based on the evolution of modes in the presence of spontaneous emission cannot only be used to analyze the noise properties of the pulse train emitted by the ML laser as usual methods, but also to analyze the fluctuations of the photon number, phase, and frequency in each mode. This allows to identify the strong noise contributions consisting in photon exchange among the HG modes. These photon number exchanges are witnesses of the particular characteristics of mode competition is among the HG modes, which is due to the relatively localized HG mode field distribution inside the cavity. The resulting noise correlations between the modes are well described by defining the noise correlation matrix. The eigenvalues and eigenvectors of this matrix permit to clearly identify the noise strength and the noise flow among the eigenmodes. The Schmidt number related to these eigenvalues allows to determine the number of eigenmodes that dominate the physical processes that the noise matrix describes.

In the presence of absorption, we investigated the evolution of different noise properties of HG modes with absorption. In terms of modes, the absorption favors mode locking, slightly reduces the mode frequency separation. It also reduces the noisy exchanges among neighbouring modes, and increases the noise in the frequency difference between modes.

Turning to the emitted pulse train, increasing the amount of saturable absorption contributes to reducing the noise in the pulse intensity, duration and timing jitter. However, this absorption should not be increased to the point where it makes mode locking unstable. Furthermore, we evaluated the phase noise of the pulse train by calculating a weighted average of the mode phase noises.

Moreover, the Henry factors of the gain and saturable absorption media are shown to reduce the mean pulse duration, but to increase the noise in pulse intensity, duration, timing jitter and phase. Finally we compared the situations where the gain and saturable absorber overlap inside the resonator and where they are located in the two opposite sides of the resonator. The noise level for separated media is generally found to be higher than when the gain and absorption overlap.

Disclosures. The authors declare no conflicts of interest.

Data availability. Data underlying the results presented in this paper are not publicly available at this time but may be obtained from the authors upon reasonable request.

Supplemental document. See Supplement 1 for supporting content.

References

1. K. C. Phillips, H. H. Gandhi, E. Mazur, and S. K. Sundaram, "Ultrafast laser processing of materials: a review," Adv. Opt. Photonics **7**(4), 684 (2015).
2. P. Ghelfi, F. Laghezza, F. Scotti, G. Serafino, A. Capria, S. Pinna, D. Onori, C. Porzi, M. Scaffardi, A. Malacarne, V. Vercesi, E. Lazzeri, F. Berizzi, and A. Bogoni, "A fully photonics-based coherent radar system," Nature **507**(7492), 341–345 (2014).
3. J. Lee, Y. J. Kim, K. Lee, S. Lee, and S. W. Kim, "Time-of-flight measurement with femtosecond light pulses," Nat. Photonics **4**(10), 716–720 (2010).
4. A. Khilo, S. J. Spector, M. E. Grein, A. H. Nejadmalayeri, C. W. Holzwarth, M. Y. Sander, M. S. Dahlem, M. Y. Peng, M. W. Geis, N. A. DiLello, J. U. Yoon, A. Motamedi, J. S. Orcutt, J. P. Wang, C. M. Sorace-Agaskar, M. A. Popović, J. Sun, G.-R. Zhou, H. Byun, J. Chen, J. L. Hoyt, H. I. Smith, R. J. Ram, M. Perrott, T. M. Lyszczarz, E. P. Ippen, and F. X. Kärtner, "Photonic ADC: overcoming the bottleneck of electronic jitter," Opt. Express **20**(4), 4454 (2012).
5. N. R. Newbury and W. C. Swann, "Low-noise fiber-laser frequency combs (Invited)," J. Opt. Soc. Am. B **24**(8), 1756 (2007).
6. S. A. Diddams, "The evolving optical frequency comb [Invited]," J. Opt. Soc. Am. B **27**(11), B51 (2010).
7. B. Bernhardt, A. Ozawa, P. Jacquet, M. Jacquey, Y. Kobayashi, T. Udem, R. Holzwarth, G. Guelachvili, T. W. Hänsch, and N. Picqué, "Cavity-enhanced dual-comb spectroscopy," Nat. Photonics **4**(1), 55–57 (2010).
8. T. Udem, R. Holzwarth, and T. W. Hänsch, "Optical frequency metrology," Nature **416**(6877), 233–237 (2002).
9. S. Gerke, J. Sperling, W. Vogel, Y. Cai, J. Roslund, N. Treps, and C. Fabre, "Full multipartite entanglement of frequency-comb Gaussian states," Phys. Rev. Lett. **114**(5), 050501 (2015).
10. Y. Cai, J. Roslund, G. Ferrini, F. Arzani, X. Xu, C. Fabre, and N. Treps, "Multimode entanglement in reconfigurable graph states using optical frequency combs," Nat. Commun. **8**(1), 15645 (2017).
11. E. U. Rafailov, M. A. Cataluna, and W. Sibbett, "Mode-locked quantum-dot lasers," Nat. Photonics **1**(7), 395–401 (2007).
12. U. Keller and A. C. Tropper, "Passively modelocked surface-emitting semiconductor lasers," Phys. Rep. **429**(2), 67–120 (2006).
13. R. M. Ma and R. F. Oulton, "Applications of nanolasers," Nat. Nanotechnol. **14**(1), 12–22 (2019).
14. G. Crosnier, D. Sanchez, S. Bouchoule, P. Monnier, G. Beaudoin, I. Sagnes, R. Raj, and F. Raineri, "Hybrid indium phosphide-on-silicon nanolaser diode," Nat. Photonics **11**(5), 297–300 (2017).
15. J. Kim and Y. Song, "Ultralow-noise mode-locked fiber lasers and frequency combs: principles, status, and applications," Adv. Opt. Photonics **8**(3), 465–540 (2016).
16. B. Lamine, C. Fabre, and N. Treps, "Quantum improvement of time transfer between remote clocks," Phys. Rev. Lett. **101**(12), 123601 (2008).

17. R. Schmeissner, V. Thiel, C. Jacquard, C. Fabre, and N. Treps, "Analysis and filtering of phase noise in an optical frequency comb at the quantum limit to improve timing measurements," Opt. Lett. **39**(12), 3603 (2014).
18. P. Jian, O. Pinel, C. Fabre, B. Lamine, and N. Treps, "Real-time displacement measurement immune from atmospheric parameters using optical frequency combs," Opt. Express **20**(24), 27133 (2012).
19. D. R. Hjelme and A. R. Mickelson, "Theory of Timing Jitter in Actively Mode-Locked Lasers," IEEE J. Quantum Electron. **28**(6), 1594–1606 (1992).
20. H. A. Haus and A. Mecozzi, "Noise of Mode-locked Lasers," IEEE J. Quantum Electron. **29**(3), 983–996 (1993).
21. H. A. Shu NamikiHaus, "Noise of the Stretched Pulse Fiber Laser: Part I—Theory," IEEE J. Quantum Electron. **33**(5), 649–659 (1997).
22. L. A. Jiang, M. E. Grein, H. A. Haus, and E. P. Ippen, "Noise of mode-locked semiconductor lasers," IEEE J. Select. Topics Quantum Electron. **7**(2), 159–167 (2001).
23. R. Paschotta, "Noise of mode-locked lasers (Part I): numerical model," Appl. Phys. B **79**(2), 153–162 (2004).
24. R. Paschotta, "Noise of mode-locked lasers (Part II): timing jitter and other fluctuations," Appl. Phys. B **79**(2), 163–173 (2004).
25. R. Paschotta, A. Schlatter, S. C. Zeller, H. R. Telle, and U. Keller, "Optical phase noise and carrier-envelope offset noise of mode-locked lasers," Appl. Phys. B: Lasers Opt. **82**(2), 265–273 (2006).
26. F. W. Helbing, G. Steinmeyer, J. Stenger, H. R. Telle, and U. Keller, "Carrier-envelope-offset dynamics and stabilization of femtosecond pulses," Appl. Phys. B: Lasers Opt. **74**(S1), s35–s42 (2002).
27. N. R. Newbury and B. R. Washburn, "Theory of the frequency comb output from a femstosecond fiber laser," IEEE J. Quantum Electron. **41**(11), 1388–1402 (2005).
28. M. C. F. Dobbelaar, S. Greveling, and D. van Oosten, "Large area photonic crystal cavities: a local density approach," Opt. Express **23**(6), 7481–7499 (2015).
29. S. Combrié, G. Lehoucq, G. Moille, A. Martin, and A. De Rossi, "Comb of high-Q Resonances in a Compact Photonic Cavity," Laser Photonics Rev. **11**(6), 1700099 (2017).
30. G. Marty, S. Combrié, A. De Rossi, and F. Raineri, "Hybrid InGaP nanobeam on silicon photonics for efficient four wave mixing," APL Photonics **4**(12), 120801 (2019).
31. G. Marty, S. Combrié, F. Raineri, and A. De Rossi, "Photonic Crystal Optical Parametric Oscillator," Nat. Photonics **15**(1), 53–58 (2021).
32. F. Alpeggiani, L. C. Andreani, and D. Gerace, "Effective bichromatic potential for ultra-high Q-factor photonic crystal slab cavities," Appl. Phys. Lett. **107**(26), 261110 (2015).
33. M. Clementi, A. Barone, T. Fromherz, D. Gerace, and M. Galli, "Selective tuning of optical modes in a silicon comb-like photonic crystal cavity," Nanophotonics **9**(1), 205–210 (2019).
34. Y. Sun, S. Combrié, F. Bretenaker, and A. De Rossi, "Mode Locking of the Hermite-Gaussian Modes of a Nanolaser," Phys. Rev. Lett. **123**(23), 233901 (2019).
35. Y. Sun, S. Combrié, A. De Rossi, and F. Bretenaker, "Dynamics of mode-locked nanolasers based on Hermite-Gaussian modes," Phys. Rev. A **102**(4), 043503 (2020).
36. Y. Sun, S. Combrié, A. De Rossi, and F. Bretenaker, "Robustness of mode-locking in harmonic cavity nanolasers subjected to potential distortions," Opt. Express **29**(4), 5782–5794 (2021).
37. B. Romeira and A. Fiore, "Purcell effect in the stimulated and spontaneous emission rates of nanoscale semiconductor lasers," IEEE J. Quantum Electron. **54**(2), 1–12 (2018).
38. J. Mørk and G. L. Lippi, "Rate equation description of quantum noise in nanolasers with few emitters," Appl. Phys. Lett. **112**(14), 141103 (2018).
39. K. Nozaki, S. Kita, and T. Baba, "Room temperature continuous wave operation and controlled spontaneous emission in ultrasmall photonic crystal nanolaser," Opt. Express **15**(12), 7506 (2007).
40. T. Wang, J. Zou, G. P. Puccioni, W. Zhao, X. Lin, H. Chen, G. Wang, and G. L. Lippi, "Methodological investigation into the noise influence on nanolasers' large signal modulation," Opt. Express **29**(4), 5081 (2021).
41. N. Takemura, M. Takiguchi, and M. Notomi, "Low- and high-β lasers in class-A limit: Photon statistics, linewidth, and the laser-phase transition analogy," J. Opt. Soc. Am. B **38**(3), 699–710 (2021).
42. A. Lebreton, I. Abram, N. Takemura, M. Kuwata-Gonokami, I. Robert-Philip, and A. Beveratos, "Stochastically sustained population oscillations in high-β nanolasers," New J. Phys. **15**(3), 033039 (2013).
43. L. A. Coldren, S. W. Corzine, and M. L. Mashanovitch, *Diode Lasers and Photonic Integrated Circuits* (John Wiley & Sons, Inc., Hoboken, NJ, USA, 2012), 2nd ed.
44. Y. Liu, Z. Wang, M. Han, S. Fan, and R. Dutton, "Mode-locking of monolithic laser diodes incorporating coupled-resonator optical waveguides," Opt. Express **13**(12), 4539–4553 (2005).
45. G. Grynberg, A. Aspect, and C. Fabre, *Introduction to quantum optics: from the semi-classical approach to quantized light* (Cambridge University Press, Cambridge, UK, 2010).
46. A. G. Vladimirov, A. S. Pimenov, and D. Rachinskii, "Numerical study of dynamical regimes in a monolithic passively mode-locked semiconductor laser," IEEE J. Quantum Electron. **45**(5), 462–468 (2009).
47. D. J. Jones, L. M. Zhang, J. E. Carroll, and D. D. Marcenac, "Dynamics of Monolithic Passively Mode-Locked Semiconductor Lasers," IEEE J. Quantum Electron. **31**(6), 1051–1058 (1995).
48. M. Heuck, S. Blaaberg, and J. Mørk, "Theory of passively mode-locked photonic crystal semiconductor lasers," Opt. Express **18**(17), 18003–18014 (2010).

49. K. A. Williams, M. G. Thompson, and I. H. White, "Long-wavelength monolithic mode-locked diode lasers," New J. Phys. **6**, 179 (2004).

50. G. L. Lippi, J. Mørk, and G. P. Puccioni, "Numerical solutions to the Laser Rate Equations with noise: technical issues, implementation and pitfalls," Proc. SPIE **10672**, 106722B (2018).

51. V. A. Averchenko, V. Thiel, and N. Treps, "Nonlinear photon subtraction from a multimode quantum field," Phys. Rev. A **89**(6), 063808 (2014).

52. C. Hönninger, R. Paschotta, F. Morier-Genoud, M. Moser, and U. Keller, "Q-switching stability limits of continuous-wave passive mode locking," J. Opt. Soc. Am. B **16**(1), 46 (1999).

53. H. R. Telle, G. Steinmeyer, A. E. Dunlop, J. Stenger, D. H. Sutter, and U. Keller, "Carrier-envelope offset phase control: A novel concept for absolute optical frequency measurement and ultrashort pulse generation," Appl. Phys. B: Lasers Opt. **69**(4), 327–332 (1999).

54. R. Paschotta, "Timing jitter and phase noise of mode-locked fiber lasers," Opt. Express **18**(5), 5041–5054 (2010).

55. A. G. Vladimirov and D. Turaev, "Model for passive mode locking in semiconductor lasers," Phys. Rev. A **72**(3), 033808 (2005).

56. S. V. Gurevich and J. Javaloyes, "Spatial instabilities of light bullets in passively-mode-locked lasers," Phys. Rev. A **96**(2), 023821 (2017).